

Numerical Simulation for Enhancement of H⁻ Production in the DC Arc-Discharge Hydrogen Negative Ion Source for Medical Use^{*)}

Shota YAMADA, Hisashi KITAMI¹⁾, Shinji NOMURA¹⁾, Yasushi AOKI¹⁾,
Kazuo HOSHINO and Akiyoshi HATAYAMA

Faculty of Science and Technology, Keio University, 3-14-1 Hiyoshi, Kohoku-ku, Yokohama 223-8522, Japan

¹⁾*Sumitomo Heavy Industries, Ltd., 19 Natsushima, Yokosuka, Kanagawa 237-8555, Japan*

(Received 9 January 2019 / Accepted 9 September 2019)

A multi-cusp DC arc-discharge hydrogen negative ion (H⁻) source has been developed for proton cyclotron, which is used for Boron Neutron Capture Therapy (BNCT). The purpose of this study is to understand the dependence of H⁻ production on the operation parameters and optimize H⁻ production in the source. In this paper, we focus on the effect of magnetic filter field on H⁻ volume production. The H⁻ density in the extraction region has been numerically estimated in the three patterns of magnetic filter field by using 3D electron transport code and 0D rate equations. The result suggests that the magnetic filter field which is localized in the vicinity of the extraction region is suitable for the efficient H⁻ volume production.

© 2019 The Japan Society of Plasma Science and Nuclear Fusion Research

Keywords: boron neutron capture therapy, hydrogen negative ion source, volume production, magnetic filter field, 3D electron transport simulation, 0D rate equation

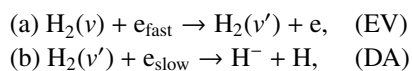
DOI: 10.1585/pfr.14.3401160

1. Introduction

A multi-cusp filament-driven DC arc-discharge H⁻ ion source has been developed for proton cyclotron, which is used for Boron Neutron Capture Therapy (BNCT). In order to shorten the treatment time of BNCT, it is required to obtain high extracted beam current from the source. The present goal of this study is to understand the dependence of H⁻ production on the operation parameters of the model H⁻ ion source [1–3] and optimize H⁻ production in the source.

The mechanisms of H⁻ production in the hydrogen plasma are mainly classified into two processes, i.e., volume production [4] and surface production [5]. Although the surface production is more efficient to obtain a large amount of H⁻ ion, it is necessary to operate an ion source with cesium seeded condition. Therefore, the H⁻ ion source is now operated as a volume production (cesium-free) type.

The volume production is mainly through the following two steps,



where ν and ν' stand for different vibrationally excitation levels ($\nu < \nu'$). The first reaction (a) is the production of vibrationally excited H₂ molecules (EV process) by the fast electrons ($E > 20$ eV), and the second reaction (b) is the H⁻ production (DA process) by the slow electrons ($E < 1$ eV).

author's e-mail: gunayama11@gmail.com

^{*)} This article is based on the presentation at the 27th International Toki Conference (ITC27) & the 13th Asia Pacific Plasma Theory Conference (APPTC2018).

In order to promote these processes, the plasma source volume is divided into two regions by the transverse magnetic field so called “magnetic filter field”. One is “driver region” where the electron temperature is high and the EV process is promoted, and the other is the extraction region where the electron temperature is low and the DA process is enhanced.

We presently focus on the effect of the magnetic filter field on the H⁻ volume production. We have already simulated the H⁻ density in the extraction region with two patterns of the magnetic filter field [6]. In order to confirm that our results are robust, the same calculation has been done with third pattern of magnetic filter field in this paper.

The simulation process mainly consists of following two steps, i) 3D electron transport analysis and ii) zero-dimensional analysis for the production of vibrationally excited H₂ molecules and H⁻ ions. In the former, the electron energy distribution function: EEDF has been calculated by KEIO-MARC code (Kinetic modeling of Electrons in the IOn source plasmas by the Multi-cusp ARC-discharge) [7–9]. In the latter, the rate equations for the vibrationally excited H₂ molecules and the particle-balance-equation for H⁻ ion have been solved.

2. The H⁻ Ion Source

Figure 1 shows a schematic drawing of the model H⁻ ion source. The source consists of a cylindrical plasma chamber made of copper, a pair of arch shaped filaments made of tungsten, permanent magnets for the multi-cusp magnetic field, dipole magnets for the magnetic filter field,

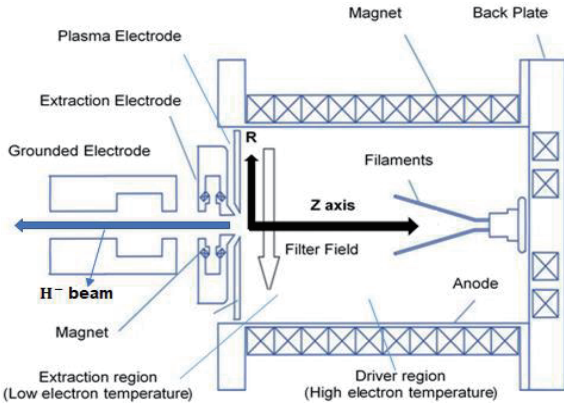


Fig. 1 Schematic drawing of the model H^- ion source [1].

and three electrodes system (PE: Plasma Electrode, EE: Extraction Electrode and GE: Grounded Electrode).

Hydrogen plasma is generated by the arc-discharge between the filaments and the chamber wall. The anode and cathode are the chamber wall and the filaments, respectively. The H^- beam is extracted from a single aperture located in the center of PE (the bottom circle of the cylindrical chamber in the extraction side). The internal radius and length of the plasma chamber are $R = 97.6$ mm and $Z = 159.1$ mm, respectively, where the origin of R and Z axis corresponds to the center of PE.

The filter magnets are located in the vicinity of PE ($Z = 0 \sim 20$ mm in the reference case) to create the magnetic filter field whose direction is perpendicular to the central axis of the chamber. As mentioned above, the chamber volume is divided by the magnetic filter field into the driver region (high energy electron region for the EV reaction) and extraction region (low energy electron region for the DA reaction).

3. Method

3.1 Magnetic filter field

The H^- density in the extraction region has been numerically estimated with three patterns of the magnetic filter field. Figure 2 shows the strength of the magnetic filter field along with Z axis with the three patterns.

The pattern A is a reference configuration of the magnetic filter field used for the present H^- source model. In the pattern B and C, the magnetic filter field is stronger than that of pattern A. In addition, the starting locations of the magnetic filter field are set to be closer to the back plate compared with pattern A. The magnetic field which can be seen in the range of $Z = 120 - 160$ mm is introduced for the plasma confinement near the back plate.

3.2 KEIO-MARC code

KEIO-MARC code is a 3D test-particle Monte-Carlo simulation model for the electron transport analysis in the multi cusp arc-discharge H^- ion sources. Realistic 3D geometries and 3D magnetic field configurations of the

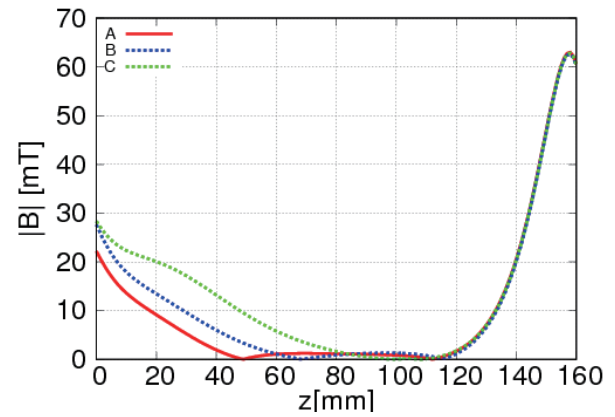


Fig. 2 Strength of magnetic filter field along with Z axis.

sources can be taken into account. KEIO-MARC code follows the trajectories of the test electrons by solving their equations of motion with the Buneman-Boris version of leap-frog method [10].

$$m_e dv_e/dt = qv_e \times \mathbf{B}, \quad (1)$$

where m_e , v_e , q , and \mathbf{B} are the electron mass, velocity, charge, and magnetic field, respectively.

The electric field is neglected under the assumption of the quasi-neutrality in the source. The quasi-neutrality condition can be valid since the Debye length becomes $10^{-4} \sim 10^{-5}$ m for the typical plasma (electron density $n_e \sim 10^{16} - 10^{18} \text{ m}^{-3}$ and electron temperature $T_e \sim 1 - 5$ eV) in the multi cusp arc-discharge H^- ion sources. The sheath potential drop at the chamber wall is, however, taken into account by using the standard formula [11]. The initial energy of the test electrons emitted from the filaments is set to be arc voltage by assuming the cathode-sheath acceleration after passing through the thin sheath layer.

In the KEIO-MARC code, collision processes are modeled by Monte-Carlo method. More than 500 elastic and inelastic collisions between electron and hydrogen species (H , H_2 , H^+ , H_2^+ , H_3^+) can be modeled by the “Null-Collision Method” [12], and the Coulomb collision is modeled by the “binary collision method” [13].

On the basis of the above model, the EEDF in the H^- source has been calculated with the three patterns of the magnetic filter field. The volume inside the plasma chamber is divided into numerical cubic cells ($2 \text{ mm} \times 2 \text{ mm} \times 2 \text{ mm}$) and the EEDF has been calculated in each cell. The arc-discharge power, voltage and H_2 gas pressure has been taken as input parameters: 2240 W, 80 V and 1.6 Pa respectively in this simulation.

As mentioned in Sec. 1, the production of the vibrationally excited H_2 molecules, which play a key role for the H^- volume production, are mainly caused by the energetic electrons ($E > 20$ eV). In order to calculate the $H_2(v)$ density and following H^- density accurately, it is important to take the non-equilibrium characteristics of the EEDF into account. Therefore, the 3D particle simulation of the elec-

tron transport explained above is essential in this study.

3.3 0D analysis of $H_2(v)$ production

The density of vibrationally excited H_2 molecule has been calculated by the 0D rate equations for each vibrational state ($0 \leq v \leq 14$).

$$\begin{aligned} dn_v/dt = & n_e n_{v'} R(eV; v' \rightarrow v) + n_e n_{v'} R(EV; v' \rightarrow v) \\ & - n_e n_v R(eV; v \rightarrow v') + n_e n_v R(EV; v \rightarrow v') \\ & - n_e n_v R(\text{diss}; v) - n_e n_v R(EV; v) \\ & - n_v n_H + R(\text{IC}; v) \\ & - \gamma n_v / \tau + S, \end{aligned} \quad (2)$$

where n_e and n_{H^+} are the electron and ion density, respectively.

Assuming the quasi-neutrality, n_{H^-} is set to be the same as n_e . This is because we assume that H^+ is the dominant positive ion in the source plasma as an initial step of this study. In the future, we need to study the population ratio of ions such as H^+ , H_2^+ , H_3^+ and H^- by solving the rate equation for these ions.

The electron density n_e can be calculated by the following equation with using the EEDF $f_e(E)$ obtained by the KEIO-MARC code,

$$n_e = \int f_e(E) dE, \quad (3)$$

where the E is the electron energy.

The density of hydrogen molecules at different vibrationally excited levels are denoted as n_v and v' . The symbols γ and τ represent the reflection rate at the chamber wall and the confinement time of H_2 molecules. The parameter γ is taken to be 0.125 for simplicity, and τ is also simply determined as L/v_{th} , where L is the radius of the plasma chamber and v_{th} is the thermal speed of H_2 molecules.

The symbol S is the gas feed for ground state of H_2 molecules which is determined by the H_2 gas pressure.

In addition, R denotes the reaction rate coefficient for each reaction process. The symbol (e.g. eV) in the parenthesis for R stands for the reaction species listed in Table 1. It should be noted that the rate coefficient R can be calculated with the EEDF $f_e(E)$ obtained by KEIO-MARC code as follows,

$$R(\text{Reac.}) = \int f_e(E) \sigma_{\text{Reac.}}(E) v_e(E) dE, \quad (4)$$

where $\sigma_{\text{Reac.}}$ and v_e are the cross section for each reaction process and the electron velocity, respectively.

As mentioned above, the production of the vibrationally excited H_2 molecules mainly occurs in the driver region. Therefore, n_e and R , which are required for solving Eq. (2), have been calculated with the EEDF obtained by averaging the EEDFs in each cell over the plane with $Z = 80$ mm in the central field free region with $0 < R < 20$ mm, as a representative of the driver region.

Table 1 Reactions which are taken into account in Eqs. (2) and (3).

	Reactions	Ref.
eV	$e + H_2(X^1\Sigma_g^+; v) \rightarrow e + H_2(X^1\Sigma_g^+; v' = v \pm 1)$	[14]
EV	$e + H_2(X^1\Sigma_g^+; v) \rightarrow e + H_2(C^1\Pi_u) \rightarrow e + H_2(X^1\Sigma_g^+; v')$	[14]
EV	$e + H_2(X^1\Sigma_g^+; v) \rightarrow e + H_2(B^1\Pi_u) \rightarrow e + H_2(X^1\Sigma_g^+; v')$	[14]
Diss	$e + H_2(X^1\Sigma_g^+; v) \rightarrow e + H_2(b^3\Sigma_u^+) \rightarrow e + H(1s) + H(1s)$	[14]
DA	$H_2(v) + e \rightarrow H^- + H$	[14]
IC	$H^+ + H_2(v) \rightarrow H(1s) + H_2^+$	[14]
ED	$H^- + e \rightarrow H + e + e$	[14]
MN	$H^- + H^+ \rightarrow H + H$	[14]
AD	$H^- + H \rightarrow H_2 + e$	[15]
NAD	$H^- + H \rightarrow H + H + e$	[15]

For initial study, we assume that the production of $H_2(v)$ molecules and transition of vibrationally excited levels are mainly caused by the collisions between electron and hydrogen molecule. Therefore, in the present model, other processes of the $H_2(v)$ production, e.g. the reverse reaction of IC; $H(1s) + H_2^+ \rightarrow H^+ + H_2(v)$ is not taken into account. In addition, the excitation and de-excitation process at the chamber wall is also neglected. In the future, however, we need to take into account these effect for more detail analysis.

3.4 0D analysis for H^- ion density

The H^- density has been estimated by the following simple 0D particle balance equation for H^- ions,

$$n_{H^-} = \frac{n_e n_v R(\text{DA}; v)}{n_e R(\text{ED}) + n_{H^+} R(\text{MN}) + n_H R(\text{AD}, \text{NAD}) + \frac{1}{\tau_{H^-}}}, \quad (5)$$

where the numerator is the H^- production rate by DA process, and the denominator is related to the loss term of H^- ions. The first three terms in the denominator are the reaction loss due to the Electron Detachment (ED), Mutual Neutralization (MN), Associative Detachment (AD) and Non-Associative Detachment (NAD), respectively, listed in Table 1. The last term of the denominator is the H^- transport loss. The symbol τ_{H^-} is the confinement time of

H^- ion. In this simulations, the τ_{H^-} is simply determined as L/v_{th} , where L is the radius of the plasma chamber and v_{th} is the thermal speed of H^- ion.

The density of vibrationally excited H_2 molecule n_v can be obtained by Eq. (2) by assuming that the H_2 density is spatially uniform inside the source. In addition, n_e and R have been calculated from the EEDF obtained by averaging the EEDFs in each cell over the length with $Z = 0-20$ mm in the central field free region with $0 < R < 20$ mm as a representative of the extraction region.

4. Results

4.1 Electron energy distribution function

In Ref. 15, the EEDF in the H^- ion source has already been calculated with the pattern A, C's magnetic filter field seen in Fig. 2. In this paper, we have newly calculated the EEDF with the pattern B. The similar result to Ref. 15 has been obtained as explained below.

The EEDF mainly consists of following two components: (i) Maxwellian components with thermal low energy electron ($E < 20$ eV) and (ii) non-equilibrium tail component with high energy electron ($E > 20$ eV). In the latter, the EEDF has a peak at $E = 80$ eV. This is because the arc-voltage is 80 V, and the initial energy of the electrons emitted from the filaments is set to be the same as the arc-voltage as mentioned in Sec. 3.2.

In the extraction region ($Z = 0-20$ mm), the non-equilibrium tail component is significantly reduced compared to that in the driver region ($Z > 80$ mm). The electron temperature in the extraction region, which can be calculated from the Maxwellian components, is also lower than that in the driver region. As mentioned above, the filter effect has clearly seen in this simulation.

4.2 Electron density

Figure 3 shows the electron density at each Z coordinate in the three patterns of the magnetic filter field. The electron density has been calculated by Eq. (3) using the averaged EEDF over the central field free region with

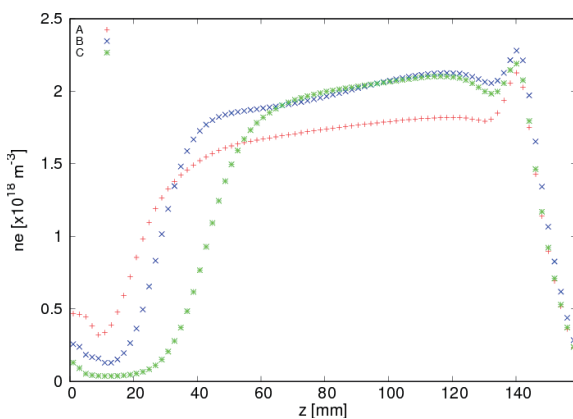


Fig. 3 The electron density at each Z coordinate.

$0 < R < 20$ mm at each Z coordinate.

The graph has a peak at $Z = 140$ mm in every pattern of the magnetic filter field. This is because there is the electron source by the filaments around $Z = 140$ mm. In the region of $Z < 140$ mm, the electron density tends to decrease with decreasing Z value due to the filter effect.

The electron density in the extraction region ($Z = 0-20$ mm), which is important for the DA process, clearly depends on the patterns of the magnetic filter field as seen in Fig. 3. The electron density averaged over the length with $Z = 0-20$ mm is $4.6 \times 10^{17} m^{-3}$ for the pattern A, $1.8 \times 10^{17} m^{-3}$ for B and $5.5 \times 10^{16} m^{-3}$ for C. The width of the magnetic filter region and its strength are the largest in the pattern C, followed by B and A in order, as seen in Fig. 2. These results suggest that the strong and widely-applied magnetic filter field reduces the electron density in the extraction region.

4.3 Density of vibrationally excited H_2 molecule

The calculation of the $H_2(v)$ density has been already done in Ref. 15 for the magnetic configurations of profile/pattern A and profile/pattern B in Fig. 2. The results show that there are no significant differences of the $H_2(v)$ density between the pattern A and B. In this paper, the same calculation has been newly done with the pattern C. The almost same result with the previous two has been obtained also in the pattern C.

4.4 H^- density in the extraction region

Table 2 shows the H^- density and electron density in the extraction region ($Z = 0-20$ mm). The H^- density is the largest for the pattern A, followed by B and C in order.

This result can be mainly explained by the electron density in the extraction region. As seen in Table 2, the dependences on the magnetic filter patterns are similar between the electron density and H^- density. Namely, the H^- density in the extraction region strongly depends on the electron density in the extraction region.

Here, we discuss the reason why such a tendency has been seen. Table 3 shows the calculated values of each term in Eq. (5). Regarding the H^- production rate $n_e n_v R(DA)$, A is the largest, followed by B and C. This result is mainly due to the difference of the electron density in the extraction region because the differences of n_v

Table 2 Electron density and H^- density in the extraction region $Z = 0-20$ mm).

	A	B	C
H^- Density [$\times 10^{16} m^{-3}$]	5.0	2.8	0.75
Electron density [$\times 10^{17} m^{-3}$]	4.6	1.8	0.55

Table 3 Electron density and H⁻ density in the extraction region
 Z = 0 - 20 mm).

	A	B	C
$n_e n_\nu R(\text{DA})$ [m ⁻³ s ⁻¹]	1.6×10^{22}	7.3×10^{21}	1.8×10^{21}
$n_e R(\text{ED})$ [s ⁻¹]	8.2×10^4	2.9×10^4	1.1×10^4
$n_{\text{H}^+} R(\text{MN})$ [s ⁻¹]	2.2×10^4	8.8×10^3	2.6×10^3
$n_{\text{H}} R(\text{AD, NAD})$ [s ⁻¹]	2.2×10^4	2.1×10^4	2.1×10^4
$1/\tau_{\text{H}^-}$ [s ⁻¹]	2.0×10^5	2.0×10^5	2.0×10^5

and $R(\text{DA})$ are much smaller than that of n_e in this calculation. The H⁻ destruction terms such as $n_e R(\text{ED})$ and $n_{\text{H}^+} R(\text{MN}) = n_e R(\text{MN})$ are also largely dependent on the electron density. Even so, the numerator of Eq. (5) which is the H⁻ production rate is more sensitive to the electron density than the denominator which is related to the H⁻ loss because of the terms which do not depend on the electron density such as $n_{\text{H}} R(\text{AD, NAD})$ and $1/\tau_{\text{H}^-}$. Due to the above reason, the H⁻ density in the extraction region strongly depends on the electron density in the extraction region.

4.5 Sensitivity of H⁻ density to the confinement time

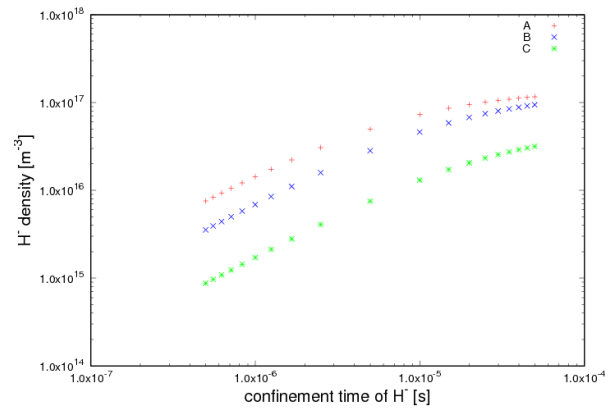
As mentioned above, the parameter τ_{H^-} is simply determined as L/v_{th} in this calculation. The radius of the plasma chamber L and the thermal speed of H⁻ ion v_{th} are 4.88×10^{-2} m and 9.79×10^3 m/s, respectively. Therefore, the reference value of τ_{H^-} becomes $\sim 5.0 \times 10^{-6}$. By considering the ambiguity of this approximation, the sensitivity of the H⁻ density to τ_{H^-} has been analyzed in the range of $\tau_{\text{H}^-} = 1/10 \times (L/v_{\text{th}}) \sim 10 \times (L/v_{\text{th}})$. Figure 4 shows the dependence of the H⁻ density on τ_{H^-} .

As can be seen in Fig. 4, the H⁻ density is the largest for the pattern A, followed by B and C at all values of τ_{H^-} . This result suggests that our simulation result of the H⁻ density in the extraction region is qualitatively robust.

The values of the H⁻ density, however, has widely changed with all patterns of the magnetic filter field. Therefore, more detailed estimation of τ_{H^-} by simulating the 3D transport process of H⁻ ion is needed for the quantitative analysis.

5. Discussion

Generally, it is believed that the role or effect of the magnetic filter field is to control the electron temperature, not the electron density.


 Fig. 4 Dependence of the H⁻ density on the confinement time of H⁻ ion.

As shown above, however, our present simulation results suggest that the difference of the electron density for the pattern A, B and C in the extraction region is the main/dominant effect of the magnetic filter. In other words, the difference of the electron density in the extraction region is more dominant effect on the H⁻ production rate and explains the resultant difference of the H⁻ density in the extraction region by the 0D analysis.

Most of the previous theoretical and simulation study of the effect of the magnetic filter field have been done with a relatively simple magnetic configuration of the filter magnetic field. More specifically, the filter magnetic field configuration exists independently with the cusp magnetic field and is modeled as a simple transverse magnetic field.

However, in reality, installing strong filter magnets affect the original multi cusp magnetic configuration, especially in the boundary region of the driver and extraction region. Electron particle and energy transport process in such a complex magnetic field configuration should be taken into account in order to obtain deeper understanding of the filter effect.

In fact, our KEIO-MARC code simulation takes into account the 3D realistic magnetic field configuration including the effects of the mutual interference between the filter field and multi-cusp magnetic field. This mutual interference makes it difficult to understand the real effect of the magnetic filter.

The role or effect of the filter field cannot be explained by previous simple modelings of the filter effect using simple magnetic configuration.

The detailed analysis of the effects of the mutual interference between the magnetic filter field and multi-cusp magnetic field on the EEDF and optimization study of the filter field configuration of the H⁻ production is beyond the scope of this paper and will be published elsewhere.

6. Conclusion

In order to understand the effect of the magnetic filter field on the H⁻ volume production, the H⁻ density in the

extraction region has been estimated with the three patterns of the magnetic filter field.

The simulation result shows that the strong and widely-applied filter field reduces the H^- density in the extraction region mainly due to the decreasing electron density in the extraction region by the filter effect. These results suggest that the magnetic filter field which is localized in the vicinity of the extraction region is suitable for the efficient H^- volume production.

7. Future Work

In the present study, however, we have used a simple 0D model for transport of the neutrals (H_2 , H) and H^- ion. Moreover, spatial profile effects have been neglected. In order to make the evaluation of the H^- density more quantitative and the present conclusion more robust, it is necessary to take into accounts these effects in the future.

- [1] H. Etoh, Y. Aoki, H. Mitsubori *et al.*, *Rev. Sci. Instrum.* **87**, 02B107 (2014).
- [2] H. Etoh, M. Onai, Y. Aoki *et al.*, *Rev. Sci. Instrum.* **87**, 02B135 (2016).
- [3] A. Hatayama *et al.*, *New J. Physics* **20**, 065001 (2018).
- [4] M. Bacal, A. Hatayama and J. Peters, *IEEE Trans. Plasma Sci.* **33**, 1845 (2005).
- [5] M. Bacal and M. Wada, *Appl. Phys. Rev.* **2**, 021305 (2015).
- [6] S. Yamada *et al.*, *AIP Conf. Proc.* (in press).
- [7] I. Fujino, A. Hatayama, N. Takado and T. Inoue, *Rev. Sci. Instrum.* **79**, 02A510 (2008).
- [8] R. Terasaki, I. Fujino, A. Hatayama, T. Mizuno and T. Inoue, *Rev. Sci. Instrum.* **81**, 02A703 (2010).
- [9] T. Shibata, M. Kashiwagi, T. Inoue, A. Hatayama and JAEA NBI Group, *J. Appl. Phys.* **114**, 143301 (2013).
- [10] C.K. Birdsall and A.B. Langdon, *Plasma Physics via Computer Simulation* (IOP Publishing, Bristol, 1991), Chap. 2, pp.12-15.
- [11] G.A. Emmert *et al.*, *Phys. Fluids* **23**, 803 (1980).
- [12] K. Nanbu, S. Igarashi and Y. Watanabe, *Proc. Soviet Union-Japan Symp. Comput. Fluid Dynamics*, (Computing Center of the USSR Academy of Sciences, 1989), Vol. 2, pp.126-132.
- [13] T. Takizuka and H. Abe, *J. Comput. Phys.* **25**, 205 (1977).
- [14] R. Celiberto, R.K. Janev, A. Laricchiuta, M. Capitelli *et al.*, *Atom. Data. Nucl.* **77**, 161 (2001).
- [15] P.T. Greenland and D. Reiter, *Juelich Report No. JUEL-3528* (1996).